Eur. Phys. J. B **66**, 301–305 (2008)
DOI: 10.1140/epjb/e2008-00441-1

THE EUROPEAN PHYSICAL JOURNAL B

High pressure Raman study of $La_{1-x}Ca_xMnO_{3-\delta}$ manganites

A. Sacchetti[1,a], T. Corridoni[2], E. Arcangeletti[3], and P. Postorino[3]

[1] Laboratorium für Festkörperphysik, ETH-Zürich, 8093 Zürich, Switzerland
[2] Dipartimento di Fisica Università di "Roma Tre", Via della Vasca Navale 84, 00146 Roma, Italy
[3] "Coherentia" CNR-INFM and Dipartimento di Fisica, Università di Roma "La Sapienza", Piazzale Aldo Moro 2, 00185 Roma, Italy

Received 18 June 2008 / Received in final form 16 September 2008
Published online 4 December 2008 –

Abstract. We report a high-pressure Raman study on two members of the $La_{1-x}Ca_xMnO_{3-\delta}$ manganite family ($x = 0.20$, $\delta = 0$ and $\delta = 0.08$). The results obtained for the $\delta = 0$ sample show a different behavior in the low and high pressure regime which is ascribed to the onset of a new pressure-activated interaction previously invoked in other manganite compounds. The comparison of our results with literature data gives further support to the identification of the Jahn-Teller sensitive stretching mode and shows that pressure-induced octahedral symmetrization is more effective in systems exhibiting a lower metallic character. On the contrary the new interaction sets in at a pressure which decreases on increasing the metallic character of the system indicating an important role of the Mn–Mn hopping integral in its activation.

PACS. 75.47.Lx Manganites – 78.30.-j Infrared and Raman spectra – 62.50.-p High-pressure effects in solids and liquids – 63.20.-e Phonons in crystal lattices

1 Introduction

The peculiar properties of colossal magneto-resistive (CMR) mixed-valence perovskite manganites [1,2] are commonly described in the framework of double exchange mechanism [3] which competes with the localizing electron-phonon coupling (EPC) triggered by the Jahn-Teller (JT) distortion of the $Mn^{+3}O_6$ octahedra[1] [4]. Nevertheless, the effects of the delicate balance among these interactions on the macroscopic properties of these systems are not yet completely understood [2]. Moreover, in recent years a number of experiments carried out on manganites under pressure pointed out the presence of a crossover from a low-pressure region, where the lattice compression favors charge delocalization, to a high pressure (HP) regime, where a new pressure-activated localizing interaction sets in and efficiently contrasts the pressure-induced enhancement of the metallic degree of the system [5–14].

Usually, pressure-induced lattice compression in CMR manganites remarkably affects the insulator to metal transition temperature, $T_{IM} \approx 200$–300 K, since the charge delocalization extent is directly related to both the EPC strength and the hopping integral. In principle, applying pressure results in an Mn–O–Mn bond length compression and consequent linearization (i.e. an increase of the hopping integral) and in a symmetrization of the JT distorted MnO_6 octahedra (i.e. a reduction of the EPC). According to the above prediction, early pressure-experiments showed an almost linear increase of T_{IM} within the $0-2$ GPa pressure range [15–21], whereas recent experiments carried out over much wider pressure ranges showed that the observed low-pressure (LP) behavior cannot be extended to the high-pressure (HP) regime. Indeed, pressure becomes progressively less effective in increasing T_{IM} and a saturation regime where T_{IM} is no more dependent on pressure, is achieved [6,7]. In several cases, when the saturation regime sets in rather early (around 4–5 GPa), further increase of pressure causes the opposite dependence with T_{IM} starting to decrease [9–13].

Among the different investigated manganite compounds, a rather complete set of HP ($0 \sim 15$ GPa) experimental data (Raman [5], Infrared [7], resistivity, X-ray [6], and neutron [22] diffraction) is available only for $La_{0.75}Ca_{0.25}MnO_3$ (LC25S). In particular, a HP Raman study of LC25S has shown a remarkable and almost linear hardening of the peak frequency of the JT-sensitive stretching mode on increasing pressure up to 7 GPa, as expected when the JT distortion is reduced. On the contrary, the peak frequency remains almost constant on further increasing the pressure up to 15 GPa [5]. A good agreement is found with X-ray diffraction data which show a pressure-induced reduction of the JT distortion over the LP regime [6]. A two-regime behavior for LC25S

[a] e-mail: sacchetti@phys.ethz.ch

[1] The crystal structure of these materials derives from the cubic perovskite structure with either a orthorhombic, rhombohedral, tetragonal, monoclinic, or hexagonal distortion.

was also observed in temperature and pressure dependent mid-infrared measurements aimed at determining the insulator-to-metal transition curve. Indeed, T_{IM} increases from 220 K to ∼300 K going from zero to ∼7 GPa but it keeps almost constant on further increasing the pressure. Additional far-infrared measurements pointed out at the failure of pressure in completely filling the insulating gap at room temperature and in leading the system towards a coherent transport regime [8]. All the data indicate the onset of the new localizing mechanism which, at room temperature, competes with the *natural* charge-delocalizing tendency of pressure and prevents both the full quenching of the JT distortion and the metallization transition. Finally, the comparison between the above experimental results and the theoretical calculations presented in reference [14] suggests the activation of an antiferromagnetic super-exchange coupling, which is in conflict with the *natural* pressure induced charge delocalization, to be responsible for the anomalous high-pressure behavior of LC25S.

In the present paper we focus on the effect of hole doping on the high-pressure behavior of CMR La–Ca manganites to gain a deeper understanding of the pressure effects and to find precursor phenomena of the localizing mechanism. Hole doping, which converts Mn^{+3} into Mn^{+4}, can be varied by changing either Ca-concentration x or oxygen stoichiometry δ in $La_{1-x}Ca_xMnO_{3-\delta}$ compounds. Indeed, since oxygen is an electron acceptor, oxygen deficiencies reduce the number of holes, which leads to an effective hole-doping $x_{eff} = x - 2\delta$. Owing to the different ionic radii of La^{3+} and Ca^{2+} (see Ref. [23]), Ca-doping induces a moderate reduction of the unit cell volume, whereas oxygen-deficiency induces negligible modifications of the average structure [24]. Exploiting oxygen non-stoichiometry it is thus possible to disentangle the effects of charge and Ca doping, provided that the configurational disorder introduced by the oxygen vacancies is not too large.

We report on high-pressure Raman measurements on two samples of $La_{0.80}Ca_{0.20}MnO_{3-\delta}$ with $\delta = 0.00$ and 0.08, which corresponds to $x_{eff} = 0.20$ and 0.04 respectively. We remark that such a large hole-density variation is accompanied by a small change in the unit cell volume (0.8% according to Ref. [25]). The stoichiometric sample has the same ground-state properties as LC25S, i.e. it is a ferromagnetic metal below Curie temperature $T_C = 194$ K, while the oxygen reduced sample is an insulator at all temperatures, with a ferromagnetic insulating phase below $T_C = 163$ K. Preparation and characterization of powder $La_{0.80}Ca_{0.20}MnO_3$ (LC20S) and $La_{0.80}Ca_{0.20}MnO_{2.92}$ (LC20D) were described in reference [25]. HP far infrared measurements on these samples were also reported in reference [8].

2 Experimental

Room temperature Raman spectra were collected using a confocal-microscope Raman spectrometer with the same experimental setup and conditions as described in reference [5]. We just recall that the low frequency cutoff of the notch filter prevents the collection of reliable spectra below 200 cm^{-1}. Sample was pressurized using a diamond anvil cell (DAC). The same sample loading procedure as in reference [5] was followed, where fine sample grains were placed on an NaCl pellet pre-sintered in the DAC and acting as pressure medium. This loading procedure prevents laser-induced sample heating [5] and ensures rather good hydrostatic conditions, as confirmed by the small linewidths of the ruby fluorescence spectrum used for the pressure calibration [26]. Small pressure gradients can anyway be present. At each pressure, four Raman spectra were collected from different points of the sample, in order to take into account these pressure gradients and to average over possible preferred orientations of the grains impinged by the laser spot, ∼10 μm^2 on the sample surface in this configuration.

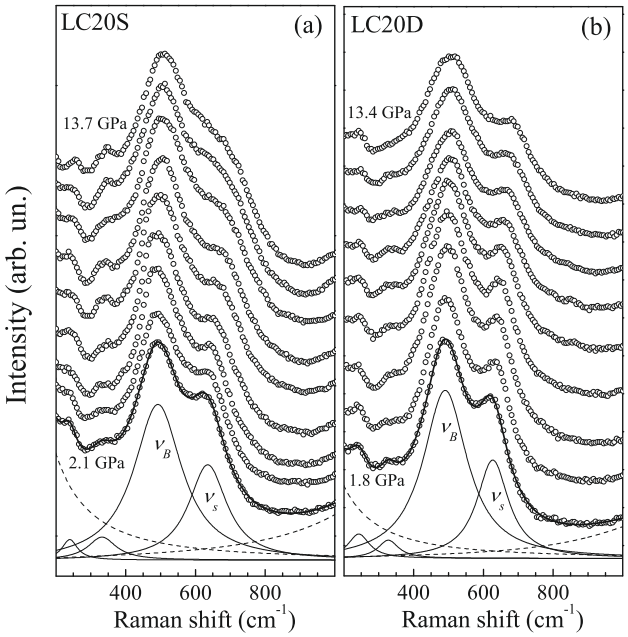

Fig. 1. Raman spectra of $La_{0.80}Ca_{0.20}MnO_3$ (LC20S, panel a) and $La_{0.80}Ca_{0.20}MnO_{2.92}$ (LC20D, panel b) at selected pressures (open symbols). Data were progressively up-shifted for clarity. Best-fit curves (thick solid line) and fitting components (solid lines: phonons, dashed lines: electronic and high frequency diamond contributions) are also shown for both samples at the lowest pressure.

3 Results and discussion

Representative Raman spectra of LC20S and LC20D collected at different pressure are shown in Figures 1a and 1b respectively. All the spectra show four rather well defined phonon peaks: $\nu_1 \sim 250$ cm^{-1}, $\nu_2 \sim 330$ cm^{-1}, $\nu_3 \sim 490$ cm^{-1}, and $\nu_4 \sim 620$ cm^{-1} at the lowest pressure. These peaks can be assigned to the octahedron modes $A_g(2)$ (b-axis rotation), $B_{3g}(4)$ (c-axis rotation), $A_g(3)$ (apical oxygen bending), and $B_{2g}(1)$ (in-plane oxygen stretching), respectively [5,27]. Although this assignment is still debated [28], in the following we refer to the

two peaks at the highest frequencies (ν_3, ν_4) as bending (ν_B) and stretching (ν_S) phonons, since further support to this assignment is here provided. The fact that the spectra of both compounds show the same overall shape and number of peaks makes us confident that the disorder introduced by oxygen vacancies has only minor effects on the lattice dynamics and adds support to the discussion below.

Raman spectra were fitted using the model curve [5]:

$$S(\nu) = [1+n(\nu)]\left[\frac{A\nu\Gamma}{\nu^2+\Gamma^2} + \sum_{i=1}^{5}\frac{A_i\nu\Gamma_i}{(\nu^2-\nu_i^2)^2+\nu^2\Gamma^2}\right] \quad (1)$$

where $n(\nu)$ is the Bose thermal population factor, while the first term in square brackets accounts for low-frequency diffusive scattering from carriers with typical lifetime Γ^{-1}. The linear combination of damped harmonic oscillators accounts for the phonon contributions and for the broad structure at around 1100 cm^{-1}, due to the diamond fluorescence background. Good fitting results were obtained for all the spectra using the model of equation (1) (see Fig. 1). At each pressure, the best-fit parameter values resulting from the analysis of the spectra collected from the four zones were averaged and the maximum dispersion value was taken as the data uncertainty. The rather small dispersion found for the best-fit values of the phonon frequency ν_i and linewidth Γ_i shows that no large pressure gradients are present. Owing to the low-frequency cutoff, the relevant parameters for the electronic contribution are affected by rather large uncertainties and do not show any defined pressure dependence. The frequency and the linewidth of the two low-frequency phonons (ν_1, ν_2 and Γ_1, Γ_2) remain constant within the uncertainty over the whole pressure range, whereas the same quantities for bending and stretching phonons (ν_B, ν_S and Γ_B, Γ_S) exhibit a remarkable pressure dependence. The pressure dependencies of ν_S and ν_B are shown in Figures 2a and 2b for LC20S and LC20D, respectively, in comparison with the corresponding data on LC25S from reference [5].

A pressure induced hardening of ν_B and ν_S frequencies is observed in all the three samples (see Fig. 2), with a pressure rate much higher for ν_S than for ν_B. Moreover, in LC20S and LC25S a two-regime behavior is well evident in the ν_S pressure dependence (i.e. linear and almost pressure independent at LP and HP, respectively).

Within the LP regime, experimental $d\nu_S/dP$ and $d\nu_B/dP$ were obtained for LC20S, LC20D and compared with literature data for LC25S [5] and for the parent compound $LaMnO_3$ [29]. It is worth to notice that the pressure derivatives in $LaMnO_3$ were obtained considering the Raman spectra up to about 8 GPa only, because the onset of a phase separation regime splits the stretching peak into two components at higher pressures [29]. The pressure derivatives are shown in the insets of Figure 2: $d\nu_S/dP$ vs. effective doping x_{eff} and $d\nu_B/dP$ vs. Ca concentration x. We remark that plotting the data vs x or x_{eff} shows a difference only for the non-stoichiometric sample LC20D ($x \neq x_{eff}$). Undoped $LaMnO_3$ ($x = x_{eff} = 0$) shows nearly the same rate for ν_S and ν_B whereas, on increasing the doping, $d\nu_S/dP$ increases and $d\nu_B/dP$ decreases.

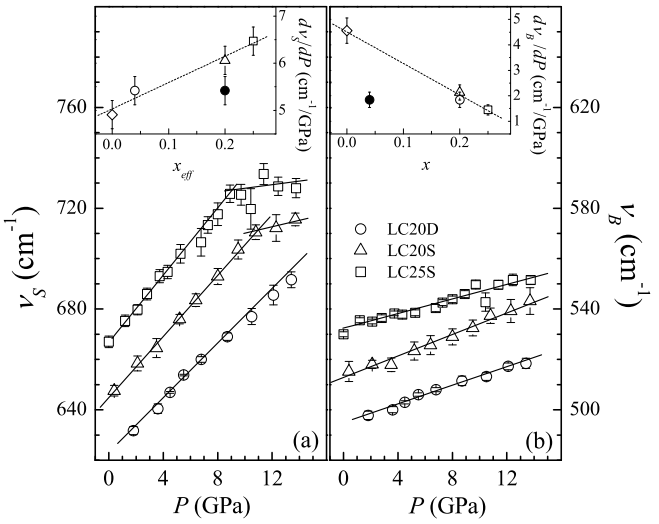

Fig. 2. Pressure dependence of phonon frequencies ν_S (a) and ν_B (b) for LC20S, LC20D, and LC25S from reference [5]. LC20S and LC25S data were up-shifted by 20 cm^{-1} and 40 cm^{-1} respectively. Insets: $d\nu_S/dP$ vs. effective doping, x_{eff} panel (a); $d\nu_B/dP$ vs. Ca-doping, x (panel b). Data for $LaMnO_3$ ($x_{eff} = x = 0$) are from reference [29]. Pressure derivatives for LC20D are also reported as a function of x in panel (a) and x_{eff} in panel (b) (filled symbols). Solid/dashed lines are guides to the eye.

Moreover, focusing on the comparison between LC20S ($x = x_{eff} = 0.20$) and LC20D ($x = 0.20$, $x_{eff} = 0.04$), it appears that $d\nu_B/dP$ depends on x and not on x_{eff}, since both the samples show the same rate $d\nu_B/dP$, whereas $d\nu_S/dP$ exhibits a linear dependence only when the data are plotted as a function of x_{eff}.

Bearing in mind that the number of Mn^{+3} centered octahedra, and thus the extent of JT distortion, is directly related to the effective charge doping x_{eff}, the above findings support the assignment of ν_S to a stretching mode strongly sensitive to the JT distortion. Moreover, since the hardening of ν_S indicates local octahedra symmetrization [5], the $d\nu_S/dP$ behavior as a function of x_{eff} indicates that, in the LP regime, pressure is more effective in reducing the JT distortion at high x_{eff}, due to the larger number of undistorted Mn^{+4} centered octahedra which make the lattice somehow *softer*. On the other hand, the pressure-induced hardening of ν_B is consistent with the assignment of the bending mode. On increasing x the average ionic radius on the rare-earth site is reduced, (La^{3+} is larger than Ca^{2+}, Ref. [23]) and the available space for bending the apical oxygen ions increases. Therefore at large x, ν_B is less affected by the pressure-induced lattice compression.

In the HP regime $d\nu_B/dP$ remains actually constant for all the samples, whereas $d\nu_S/dP$ almost vanishes above 7 GPa and 9 GPa for LC25S and LC20S respectively. No saturation effects were observed for LC20D over the explored pressure range. The difference between the LP and HP regimes is ascribed to the onset of a new pressure-activated mechanism competing with the pressure induced

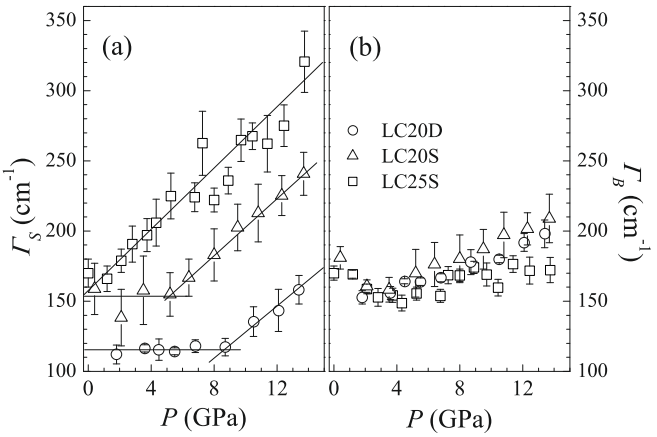

Fig. 3. Pressure dependence of the linewidth Γ_S (a) and Γ_B (b) of the stretching and the bending modes respectively, for LC20S and LC20D, compared with results on LC25S from reference [5]. Solid lines are guides to the eye.

symmetrization of the MnO_6 octahedra [5,6]. Since the threshold pressure for the activation of the pressure-activated mechanism appears to decrease on increasing x_{eff}, that is on increasing the metallic character of the system, this finding suggests that the new interaction could be somehow related to the effective Mn–Mn hopping integral, rather than to steric effects. These results are in agreement with far infrared measurements [8] on the same three samples showing that, in samples with metallic ground state, the pressure-induced charge-delocalization process is much more pronounced in LC20S, which exhibits a smaller $T_C = T_{IM}$ and a larger gap at $P = 0$, while at HP both LC20S and LC25S seem to approach the same regime.

The onset of the localizing mechanism can be seen also in the pressure dependencies of the linewidths of the bending (Γ_B) and stretching (Γ_S) phonons of LC20S and LC20D shown in Figures 3a and 3b, respectively, and compared with corresponding results on LC25S from reference [5]. LC25S shows the largest Γ_S and LC20D the smallest, whereas Γ_B is almost identical in all the three samples. This effect can be interpreted in terms of the disorder of the JT distortion induced by hole doping and it is more evident in LC25S where x and x_{eff} are larger. We notice that, since measurements have been carried out on sample grains on the micron scale, spurious broadening of the phonon peaks and little effects on the peak frequencies can be induced by small variation of the oxygen stoichiometry at grain boundaries. Nevertheless grain effects should induce similar modifications on all the samples and on both the stretching and the bending bands. The remarkably different behavior under lattice compression shown by the ν_S and ν_B phonon peaks makes us confident that, at least, the pressure dependencies obtained are mainly due to intrinsic properties of the samples and not to spurious effects. In particular the weak pressure dependence of the Γ_B values, almost identical in all the measured samples, in comparison with the strong dependencies shown by Γ_S values, clearly different in each sample, suggests that the bending phonon is weakly correlated to carrier density and thus to the extent of JT distortion.

A two-regime behavior can be envisaged for Γ_S: on increasing pressure, at first the linewidth remains constant and, above a threshold, it starts to increase linearly. A threshold value of ∼8 GPa is rather apparent for LC20D whereas it can be roughly evaluated at around 5 GPa for LC20S. In the case of LC25S we can say that the threshold goes to zero and the linewidth linearly increases starting from ambient pressure. The onset of the lineshape broadening could be a precursor of the saturation regime shown by the pressure dependence of ν_S. The linewidth behavior is consistent with the onset of a new interaction in the HP regime, which reduces the phonon life-time and thus broadens the peak. Since the effect of pressure is on one side to reduce JT distortion and on the other side to activate a localizing interaction, a large dispersion of the extent of JT distortion or even the coexistence of distorted and undistorted octahedra is expected. With this respect we would like to recall that the coexistence of domains of JT distorted and almost regular MnO_6 octahedra in $LaMnO_3$ ($x = x_{eff} = 0$) has been deduced from the observed splitting of the stretching mode at pressures above 8 GPa i.e. at a pressure very close to the threshold pressure above which Γ_S of LC20D ($x_{eff} = 0.04$) starts to increase.

We finally notice that, although very similar, the Raman spectra of doped (and/or oxygen-deficient) compounds show a remarkable disorder-induced broadening of lineshapes [30] with respect to that of $LaMnO_3$. Namely at $P = 0$, Γ_S of LC20D is more than twice Γ_S of $LaMnO_3$ thus avoiding to resolve a possible fine structure of the stretching peak expected if phase-separation occurs.

4 Conclusions

In summary, we reported on high-pressure Raman measurements on $La_{0.80}Ca_{0.20}MnO_{3-\delta}$ with $\delta = 0.00$ and 0.08. A careful analysis of the phonon pressure dependence as a function of Ca and effective charge doping provided further support to the assignment of the bending and the JT-sensitive stretching octahedral modes. Moreover our results give spectroscopic evidence of the onset of a localizing mechanism at HP in metallic ground state manganites, confirming and extending previous data on $La_{0.75}Ca_{0.25}MnO_3$ [5]. The comparison of the present results with literature data allows us to evidence that the greater the metallic degree of the system, the smaller the pressure at which the localizing interaction effect sets in, demonstrating that the strength of the new localizing interaction depends on the effective Mn–Mn hopping integral, which increases on increasing x_{eff}, as well as on increasing pressure. This results is in agreement with the theoretical scenario proposed in reference [14], in which the localizing super-exchange antiferromagnetic coupling becomes competitive with double exchange at HP.

The authors wish to thank D. Emin for providing the samples studied in the present work.

References

1. A.J. Millis, Nature **392**, 147 (1998)
2. E. Dagotto, *Nanoscale Phase Separation and Colossal Magnetoresistance* (Springer-Verlag, Berlin, 2002)
3. C. Zener, Phys. Rev. **82**, 403 (1951)
4. A.J. Millis, P.B. Littlewood, B.I. Shraiman, Phys. Rev. Lett. **74**, 5144 (1995)
5. A. Congeduti, P. Postorino, E. Caramagno, M. Nardone, A. Kumar, D.D. Sarma, Phys. Rev. Lett. **86**, 1251 (2001)
6. C. Meneghini, D. Levy, S. Mobilio, M. Ortolani, M. Nuñez-Reguero, A. Kumar, D.D. Sarma, Phys. Rev. B **65**, 012111 (2002)
7. P. Postorino, A. Congeduti, P. Dore, A. Sacchetti, F.A. Gorelli, L. Ulivi, A. Kumar, D.D. Sarma, Phys. Rev. Lett. **91**, 175501 (2003)
8. A. Sacchetti, M.C. Guidi, E. Arcangeletti, A. Nucara, P. Calvani, M. Piccinini, A. Marcelli, P. Postorino, Phys. Rev. Lett. **96**, 35503 (2006)
9. C. Cui, T.A. Tyson, Z. Zhong, J.P. Carlo, Y. Qin, Phys. Rev. B **67**, 104107 (2003)
10. C. Cui, T.A. Tyson, Appl. Phys. Lett. **83**, 2856 (2003)
11. C. Cui, T.A. Tyson, Z. Chen, Z. Zhong, Phys. Rev. B **68**, 214417 (2003)
12. C. Cui, T.A. Tyson, Appl. Phys. Lett. **84**, 2856 (2004)
13. C. Cui, T.A. Tyson, Phys. Rev. B **70**, 094409 (2004)
14. A. Sacchetti, P. Postorino, M. Capone, N.J. Phys **8**, 3 (2006)
15. P.G. Radaelli, G. Iannone, M. Marezio, H.Y. Hwang, S-W. Cheong, J.D. Jorgensen, D.N. Argyriou, Phys. Rev. B **56**, 8265 (1997)
16. Y. Moritomo, H. Kuwahara, Y. Tokura, J. Phys. Soc. Jpn **66**, 556 (1997)
17. H.Y. Hwang, T.T.M. Palstra, S.-W. Cheong, B. Batlogg, Phys. Rev. B **52**, 15046 (1995)
18. J.J. Nuemeier, M.F. Hundley, J.D. Thompson, R.H. Heffner, Phys. Rev. B **52**, R7006 (1995)
19. K. Kamenev, G. Balakrishnan, M.R. Lees, D. McK. Paul, Z. Arnold, O. Mikulina, Phys. Rev. B **56**, 2285 (1997)
20. Y.S. Wang, A.K. Heilman, B. Lorenz, Y.Y. Xue, C.W. Chu, J.P. Franck, W.M. Chen, Phys. Rev. B **60**, R14998 (1999)
21. B. Lorenz, A.K. Heilman, Y.S. Wang, Y.Y. Xue, C.W. Chu, G. Zhang, J.P. Franck, Phys. Rev. B **63**, 144405 (2001)
22. D.P. Kozlenko, S.E. Kichanov, V.I. Voronin, B.N. Savenko, V.P. Glazkov, E.A. Kiseleva, N.V. Proskurnina, JETP Lett. **82**, 447 (2005)
23. R.D. Shannon, Acta Crystallogr. A **32**, 751 (1976)
24. I.O. Troyanchuk, S.V. Trukhanov, H. Szymczak, J. Przewoznik, K. Bärner, J. Exp. Theor. Phys. **93**, 161 (2001)
25. T.L. Aselage, D. Emin, S.S. McCready, E.L. Venturini, M.A. Rodriguez, J.A. Voigt, T.J. Headley, Phys. Rev. B **68**, 134448 (2003)
26. H.K. Mao, J. Xu, P.M. Bell, J. Geophys. Res. **91**, 4673 (1986)
27. M.N. Iliev, M.V. Abrashev, H.G. Lee, V.N. Popov, Y.Y. Sun, C. Thomsen, R.L. Meng, C.W. Chu, Phys. Rev. B. **57**, 2872 (1998)
28. M.N. Iliev, M.V. Abrashev, J. Raman Spectrosc. **32**, 805 (2001)
29. I. Loa, P. Adler, A. Grzechnik, K. Syassen, U. Schwarz, M. Hanfland, G.K. Rozenberg, P. Gorodetsky, M.P. Pasternak, Phys. Rev. Lett. **87**, 125501 (2001)
30. P. Postorino, A. Congeduti, E. Degiorgi, J.P. Itié, P. Munsch, Phys. Rev. B. **65**, 224102 (2002)